HHS Public Access

Author manuscript

Nat Med. Author manuscript; available in PMC 2019 August 18.

Published in final edited form as:

Nat Med. 2019 March ; 25(3): 427–432. doi:10.1038/s41591-019-0344-3.

Long-term Evaluation of AAV-CRISPR Genome Editing for Duchenne Muscular Dystrophy

Christopher E. Nelson[1,2], **Yaoying Wu**[1], **Matthew P. Gemberling**[1,2], **Matthew L. Oliver**[1], **Matthew A. Waller**[1,2], **Joel D. Bohning**[1,2], **Jacqueline N. Robinson-Hamm**[1,2], **Karen Bulaklak**[1,2], **Ruth M. Castellanos Rivera**[3], **Joel H. Collier**[1], **Aravind Asokan**[4,5], and **Charles A. Gersbach**[1,2,6,*]

[1]Department of Biomedical Engineering, Duke University, Durham, North Carolina, United States of America

[2]Center for Genomic and Computational Biology, Duke University, Durham, North Carolina, United States of America

[3]Gene Therapy Center, University of North Carolina Chapel Hill, Chapel Hill, North Carolina, United States of America

[4]Department of Surgery, Duke University Medical Center, Durham, North Carolina, United States of America

[5]Department of Molecular Genetics & Microbiology, Duke University Medical Center, Durham, North Carolina, United States of America

[6]Department of Orthopaedic Surgery, Duke University Medical Center, Durham, North Carolina, United States of America

*Corresponding author Address for correspondence: Charles A. Gersbach, Ph.D., Department of Biomedical Engineering, Room 1427, FCIEMAS, 101 Science Drive, Box 90281, Duke University, Durham, NC 27708-0281, charles.gersbach@duke.edu.

Contributions: C.E.N. designed and conducted experiments, Y.W. provided expertise on immune experiments including Elispot, M.P.G. conducted experiments and mouse procedures, M.L.O. produced protein and histology, M.A.W. completed qPCR experiments, J.D.B. performed histological analyses, J.N.R.-H. performed creatine kinase assays, K.B. performed mouse procedures, R.M.C.R. produced recombinant AAV, A.A., J.H.C., and C.A.G. designed experiments, C.E.N. and C.A.G. wrote and revised the manuscript.

Reporting summary

The life sciences reporting summary is linked to the online version of this article with additional detail on experimental design and reproducibility.

Conflict of Interest

JNRH, CEN, and CAG have filed patent applications related to genome editing for Duchenne muscular dystrophy. CAG is an advisor to Sarepta Therapeutics, and a co-founder and advisor to Element Genomics and Locus Biosciences. AA is a co-founder and advisor to StrideBio.

Data Availability

All custom code for reproducing Figures 1C–D, 3B, 3D, 4A–D have been made available at online (https://github.com/chrisnelsonlab/CRISPR-Nextera/). All sequencing data used in this study has been deposited in the National Center for Biotechnology Information Sequence Read Archive (SRA) database (SRP157083). Full uncropped gels are included as source data. All other relevant raw data are available from the corresponding author on request.

Introductory Paragraph

Duchenne Muscular Dystrophy (DMD) is a monogenic disorder and a candidate for therapeutic genome editing. There have been several recent reports of genome editing in preclinical models of DMD [1–6], however, the long-term persistence and safety of these genome editing approaches have not been addressed. Here we show that genome editing and dystrophin protein restoration is sustained in the mdx mouse model of DMD for one year after a single intravenous administration of AAV-CRISPR. We also confirmed immunogenic properties of AAV-CRISPR when administered to adult mice [7], but show that the humoral and cellular immune response can be avoided by treating neonatal mice. Additionally, we show unintended genome and transcript alterations induced by AAV-CRISPR that should be considered for the development of AAV-CRISPR as a therapeutic approach. This study shows the potential of AAV-CRISPR for permanent genome correction and highlights aspects of host response and alternative genome editing outcomes for further study.

Main

Duchenne muscular dystrophy (DMD) is a debilitating and prematurely fatal genetic disease caused by mutations in the *DMD* gene leading to the absence of dystrophin [8, 9]. Despite recent clinical advancements [10, 11], a curative approach remains elusive. Adeno-associated virus (AAV) is being used as a gene delivery vector for recently initiated DMD clinical trials and for two approved gene therapy products and has been tested in more than 100 clinical trials [12]. Multiple groups are using AAV to deliver genome editing technologies to make permanent genetic modifications to treat disease, including the first human genome editing clinical trial using AAV that is currently underway using zinc finger nuclease technology [13, 14]. Genome editing has been used to repair the *DMD* gene by exon deletion [1–6], splice-site targeting [15], or homology directed repair (HDR) [6] in mouse models of DMD and most recently in a canine model of DMD [16]. These studies show genome editing restores dystrophin expression in mouse models of DMD leading to an improvement in skeletal muscle function. The enthusiasm for a genome editing strategy is founded on the potential for a single administration for life-long therapeutic benefit. However, published studies have focused on short-term restoration of dystrophin, typically assessed at 4–8 weeks post-treatment. In this study, we treated mice with a dual-AAV system, one AAV encoding CRISPR-Cas9 and the other AAV encoding two gRNAs designed to excise exon 23 from the *Dmd* gene in mdx mice. For viral packaging, we used the smaller 3.2 kb Cas9 derived from *Staphylococcus aureus* (SaCas9) [17]. We examined both AAV serotype 8 (AAV8) and AAV9 (Fig. 1A–B) which have differential tissue tropism for heart, skeletal muscle, and liver in animal models that are not perfectly predictive of human tropism [18]. We examined adult and P2 neonatal mice treated locally by intramuscular (IM) injection and systemically by intravenous facial-vein injection (FVI), respectively for restoration of dystrophin expression (Fig. 1A–B). We adapted an unbiased deep-sequencing method for precise quantification of gene editing efficiencies. Mice injected IM as adults had a significant decrease in genome editing levels over time (Fig. 1C, Extended Data Fig. 1). In contrast, systemically treated mice had a modest statistically significant increase in genome editing levels over one year (Fig. 1D, Extended Data Fig. 1). The SaCas9 expression cassette was driven by a constitutive CMV promoter that is

expressed in multiple muscle cell types including striated muscle and muscle progenitors [5]. However, genome editing events were also detected in other tissues including liver, spleen, kidney, and brain, as well as the testis at levels barely above the limit of detection (~0.1%, Extended Data Fig. 2). Use of a myocyte-specific promoter could restrict editing to striated muscle nuclei [6], but potentially at the cost of editing muscle progenitor cells. Analysis of *Dmd* mRNA transcripts by droplet digital PCR (ddPCR) showed the same trend as the genomic deletions with significant increases over time noted in cardiac muscle from systemically treated mice (Fig.1E–F). Sustained dystrophin protein restoration was detected by immunofluorescence staining and western blot of cardiac and skeletal muscle from systemically treated mice for at least one year after a single administration (Fig. 1G–H, Extended Data Fig. 3). The restored dystrophin was slightly smaller in younger mice than older mice, potentially due to a smaller protein isoform produced at the early time point while nearly full-length dystrophin was detected at one year. Serum creatine kinase levels were reduced at 8 weeks post-treatment in mice treated systemically as neonates, demonstrating protection from muscle damage by the restored dystrophin protein (Fig 1I). Deep sequencing of the top ten predicted off-target sites showed no significant increase in off-target cutting after one year with slight activity above background noted for gRNA1 at off-target site #8 (gRNA1-OT8), as was previously identified following local administration (Table S1–2) [4].

An important consideration to long-term therapeutic benefit of *in vivo* genome editing is the host response to bacteria-derived Cas9 proteins. In our study, a humoral immune response was detected against the SaCas9 protein in nearly all mice injected as adults (N=31/32, Fig 2A, Extended Data Fig. 4). In contrast, no humoral response against SaCas9 was detected in mice treated as neonates by facial vein injection or intraperitoneal injections (N=0/19, Fig. 2A). A cellular response was detected by re-stimulation with SaCas9 to produce IFNγ-secreting T cells in mice treated as adults but not neonates, regardless of administration route (Fig 2B, Extended Data Fig. 4). The mdx mouse model has an increased baseline number of infiltrating macrophages and neutrophils due to muscle degeneration and inflammation [19], which treatment with AAV-CRISPR has been shown to decrease [4]. Expression of FoxP3, GM-CSF, IL1β, and IL12β decreased relative to untreated mdx mice after IM injection, however, IFNγ significantly increased ~7 fold after local injection relative to untreated mdx mice (Extended Data Fig. 4). In contrast, systemically treated adults and neonates showed no significant changes in these markers of inflammatory cell infiltration. Most AAV vector genomes remain episomal after cell entry and are stably maintained in non-dividing cells [20]. In this study, AAV vectors persisted between eight weeks and one year in cardiac muscle but were significantly lost in skeletal muscle after IM or FVI injection (Fig. 2C–D). Regardless, expression of SaCas9 mRNA and both gRNAs is virtually absent after six months or one year by either route of administration (Fig. 2E–F) which may be the result of promoter silencing [21]. The host response to AAV-CRISPR will need to be carefully considered for future clinical development, including pre-existing immunity in humans [22]. We have previously shown CRISPR-based gene silencing elicits a Cas9-dependent host response that resolves without intervention *in vivo* [23]. Our data here indicates that a significant host response is avoided if AAV-CRISPR is administered to neonates. Although the two day-old mice have an undeveloped immune system which can be

exploited for antigen-specific tolerance including Cas9 [24–26], it is not yet clear to what extent this approach could apply in newborn humans. Other methods that could be explored to avoid anti-Cas9 immune response include transient immunosuppression for the length of vector expression, induction of immune tolerance [27], removal of T cell epitopes [28], or use of self-limiting/cleaving vectors or other transient delivery vehicles including non-viral vectors [29].

The methods used to assess *in vivo* genome editing efficiencies have typically been designed to quantify the frequency of expected genome editing outcomes. Additionally, different methods often must be used to quantify the various possible editing outcomes. For example, PCR-based methods for deep sequencing can detect indel formation after genome editing but cannot quantify gene deletions and do not capture larger structural changes that remove one or both primer sites. Previously, we used ddPCR to quantify genetic changes including deletions [4] but ddPCR requires separate priming strategies to amplify each gene editing outcome, including unedited alleles and different editing events, and cannot detect unexpected events. To comprehensively map all possible genome editing outcomes with an unbiased approach, we adapted Illumina's Nextera-transposon-based library preparation method for unbiased sequencing [30]. This method used a single genome-specific forward primer for target enrichment and a reverse primer specific for the DNA tag integrated by the transposon. In addition to genomic deletions, this method is sensitive to indel formation, inversion of exon 23 and surrounding introns, and integration of the AAV genome (Fig 3A). With this method we show quantifiable and heterogenous genome editing events at the on-target *Dmd* locus that have not been previously reported, including deletions, inversions, indels, and AAV integrations in all treated mice (Fig. 3B, Extended Data Fig. 5). Importantly, no chromosomal translocations driven by off-target DNA cutting were detected in this experiment (estimated limit of detection ~0.01%, Extended Data Fig. 5). The majority of deletion events were perfect deletions consistent with previous observations [4, 31]. We detected a low prevalence (<0.5%) of large asymmetrical deletions (Fig. 3C, Table S3) consistent with a previous report using long-read sequencing to monitor genome editing outcomes in pluripotent cells *in vitro* [32], however, our method cannot detect large deletions that remove both primer sites. The sequencing method used here is reproducible and matches indel quantification collected through a more standard next-generation sequencing method (Extended Data Fig. 6). We also applied this Nextera-based sequencing approach to cDNA of treated mice. This approach is sensitive to exon 23 removal and unexpected transcript changes including aberrant splicing (Fig. 3D, Extended Data Fig. 7). We detected removal of exon 23, changes in splicing including multi-exon skipping, putative circular RNA formation, and AAV splicing events (Fig. 3E, Table S4–S5). Splicing events with the AAV vector genome contained canonical splice acceptors or donors (Extended Data Fig. 8, Table S6). Multi-exon skipping may lead to partially functional or dysfunctional protein depending on the change to the reading frame. The circular RNAs do not resemble a functional mRNA and will not be translated into protein, and therefore are expected to have little biological significance. The relative enrichment of circular RNAs seen here may be caused by the stability of circular RNAs against exonuclease activity [33]. Transcript isoforms containing partial AAV genomes have an unknown biological effect. The levels of exon 23 excision determined by this sequencing method are comparable to the results

obtained by ddPCR analysis for quantification of exon 23 removal (Extended Data Fig. 8). Sequencing of the cDNA isolated at different time points indicated that the transcript isoform levels are sustained over one year (Extended Data Fig. 7).

AAV is being used extensively as a delivery vector for CRISPR-Cas9 in preclinical studies to treat inherited diseases including DMD [1, 34]. While the safety of AAV as a gene delivery vehicle has been shown preclinically and through over 100 clinical trials, the potential genotoxicity of the combination of AAV and CRISPR requires more characterization. Here we adapted next-generation sequencing modalities to characterize unintended genome editing events and AAV genome integrations. In this study, AAV typically integrated within the viral ITRs (62%) resembling canonical integration [35], however, insertions within the viral genome were also detected (38%) (Fig. 4A). Insertions that occur internally within the vector genome may be the result of vector truncations from AAV packaging or from AAV genome insertion during DNA repair. Separately, a primer specific for the AAV vector genome was used in conjunction with the same transposon-specific primer to map genome-wide AAV vector episome integration into the mouse genome (Fig 4B). This showed that the targeted site within the *Dmd* gene was the preferential location for integration in both neonatal liver and cardiac muscle. In tissues that were analyzed eight weeks after systemic delivery to neonatal mice, 94 AAV integration sites were identified in liver and 72 sites in cardiac muscle with the majority of integration events occurring within introns of genes consistent with previous observations including several previously identified integration sites (Fig. 4C, Table S7) [36]. Several putative gRNA off-target sites were also identified by AAV integration (Fig. 4B – red, Fig. 4D), including a previously predicted off-target site in an intergenic region of chromosome 14 for which there was no detectable activity by conventional targeted deep sequencing in the same samples (Fig. 4C, site #6) [4]. This suggests that unbiased mapping of AAV integrations may be a more sensitive approach to determining specificity of genome editing reagents than typical methods.

In this study, the frequency of AAV integrations into the CRISPR-induced double-strand break was higher than the intended deletion (Fig. 3B). AAV integration into targeted DSBs was reported more than a decade ago [35] and also applied as a therapeutic gene therapy approach [14]. AAV can integrate into random breaks across the genome by non-homologous end-joining and can also be copied into target loci by homologous recombination without expression of nucleases [37]. Preclinical reports of hepatocellular carcinoma caused by genotoxicity of the vector have been controversial and risks can be managed by vector design [36, 38–40]. AAV is currently the gene delivery vehicle for more than 100 clinical trials targeting liver, skeletal muscle, cardiac muscle, central nervous system, and other tissues with no reported adverse events caused by genotoxicity of the vector. However, the induction of a novel DNA break by any genome editing construct could potentially change the integration landscape and genotoxicity profile of AAV (Fig. 4B–D). Additionally, each genome engineering construct will have different genome-wide insertional mutagenesis profiles and should be carefully considered when developing vectors for therapeutic genome editing. Preclinical work can monitor *cis* activation of oncogenes and clonal expansion of AAV integration sites to reduce potential genotoxicity risks of genome

editing technologies delivered by AAV [36], analogous to efforts to characterize lentiviral vector integration, which also has an excellent safety profile in human clinical trials.

Important for future preclinical development will be focused on increasing the overall editing efficiency and increasing the proportion of the intended gene modification by optimizing delivery and the gene editing strategy. This study further establishes the feasibility of permanent gene correction as a therapeutic approach for DMD and potentially other diseases. Despite the presence of a host response to Cas9 and persistent unintended genome modifications, AAV-CRISPR was well-tolerated for one year with no sign of toxicity, though much larger studies are required to confirm the absence of genotoxicity risk. Moreover, the restoration of dystrophin expression was sustained over this period. New developments to characterize safety and efficiency in larger animal models and mitigate the potential immune response will be crucial to translate this technology to treat genetic disease.

Online Methods

AAV preparation

SaCas9 and gRNA containing AAV constructs were generated as previously described [4]. Briefly, a Staphylococcus aureus Cas9 (SaCas9) expression plasmid with a CMV promoter containing ITRs and a plasmid containing two gRNA expression cassettes driven by the human U6 polIII promoter were used to prepare recombinant AAV8 and AAV9. ITRs were confirmed by SmaI digest before AAV production. Multiple batches of AAV8 and AAV9 were produced and titers measured by qPCR as previously described.

In vivo administration of AAV-CRISPR

All experiments involving animals were conducted with strict adherence to the guidelines for the care and use of laboratory animals of the National Institute of Health (NIH). All experiments were approved by the Institutional Animal Care and Use Committee (IACUC) at Duke University. The mouse strain C57BL/10ScSn-Dmdmdx/J (*mdx*) was obtained from Jackson labs. C57BL/10 were used as a wild-type control. Adult 8-week-old male mice were administered locally into the tibialis anterior muscle with 30uL of 5.6×10^{11} vg/vector/mouse. Adult 8-week-old mice were administered intravenously with 200uL injections of 2.7×10^{12} vg/vector/mouse. Two-day-old (P2) neonatal mice were administered intravenously through the facial vein [41] with 5.4×10^{11} vg/vector/mouse. At set time points (Fig. 1A) mice were harvested for multiple skeletal muscles, cardiac muscles, other organs, and serum.

Genomic DNA extraction and next-generation sequencing

Genomic DNA was extracted from various mouse tissues at defined time points by digestion in proteinase K and ALT buffer at 56°C overnight while shaking. DNA was further extracted with the DNeasy kit (Qiagen). Endpoint PCR to confirm deletion was performed with AccuPrime Polymerase (Invitrogen) using primers DMDin22F/DMDin23R (Table S8). Indel formation was detected by next-generation sequencing. Amplicons were produced by PCR using AccuPrime Polymerase (Invtrogen) and a series of primers for each locus (Table S8).

A second short-cycle PCR was used to add Illumina flowcell binding sequences and experiment-specific barcodes (Table S8). The resulting PCR products were sequenced with 150bp paired-end reads on an Miseq instrument (Illumina). Indel analysis was performed using a local distribution of CRISPResso Pooled [42] using a 5bp window and standard settings.

Transposon-mediated target enrichment and sequencing

100 ng – 1 μg of genomic DNA was tagmented using a Nextera Tn5 transposon (Illumina) following manufacturer's instructions except with the transposon diluted 1:8 from specifications to encourage large fragment size (Extended Data Fig. 9). To enrich the targeted sequence, a single PCR reaction using a genome specific primer (DMDin22-Nextera-F) or (DMDin23-Nextera-R) was used paired with a reverse primer specific for the tag sequence inserted by the transposon (Nextera-R) for 25 cycles. Amplicons were purified with Ampure beads (Beckman Coulter) at 1.8x. A short 10-cycle PCR was used to add experimental barcodes and Illumina adapter sequences. Amplicons were gel purified selecting the fragment size shown in Extended Data Fig. 9. Sequencing was conducted on an Illumina Miseq using v2 chemistry and a 2×150 cycle paired end reads. Analysis was performed by aligning amplicons to the targeted locus and discarding mis-primed sequences. Targeted amplicons range from 5–40% depending on the primer used (Extended Data Fig. 9). Reads were then aligned to expected products including deletions, inversions, AAV integrations, and genome-wide translocations. Alignments to the AAV genome (Fig. 4A) used Needleman-Wunsch algorithm with a GapOpenValue of 10. Some reads within the AAV ITRs were ambiguous and were randomly assigned to one of the two ITRs for alignment. This Nextera-based method is expected to reduce PCR-related bias from amplicon size, however some bias may remain for the transposon selectivity [30].

Transcript evaluation and sequencing

RNA was extracted using the Qiagen Universal kit. 1 μg was used to perform First-strand cDNA synthesis using Vilo kit (ThermoFisher) according to manufacturer's instructions. cDNA was diluted 1:4 in ultrapure water aliquoted and stored for further analysis. For transposon-based sequencing, second strand cDNA synthesis was performed using Klenow fragment DNA polymerase (NEB). cDNA was treated with Nextera Tn5 transposon at 1:8 recommended concentration. Enrichment of the target transcript was performed by PCR using transcript specific primers (Ex22-Nextera-F or Ex24-Nextera-R) and a constant reverse primer specific for tag inserted by the transposon (Nextera-R). Amplicons were purified by Ampure beads at 1.8x and a second 10-cycle PCR was used to add adapters and barcodes. Reads were aligned to predicted amplicons and mis-aligned reads were discarded. Reads were then aligned to expected products and unexpected products were identified and quantified. qPCR was conducted using QuantaBio PerfeCTa SYBR® Green SuperMix using the primers listed in Table S8.

Western blot

Frozen muscle biopsies were disrupted with mortar and pestle and suspended in RIPA buffer (Sigma) with a proteinase inhibitor cocktail (Roche) and incubated for 30 min on ice with intermittent vortexing. Samples were centrifuged at 16,000 x g for 30 min at 4°C and the

supernatant was isolated and quantified with a bicinchoninic acid assay (Pierce). Protein isolate was mixed with NuPAGE loading buffer (Invitrogen) with 5% β-mercaptoethanol and boiled at 100°C for 10 min. Samples were flash frozen in liquid nitrogen and stored at −80°C. 25 μg of total protein per lane was loaded into a 10 well 4–12% NuPAGE Bis-Tris gel (Invitrogen) with MES buffer (Invitrogen) and electrophoresed for 30 min at 200V. Protein was transferred to a nitrocellulase membrane for 1 hour at 400 mA at 4°C in transfer buffer containing 1X tris-glyceine, 10% methanol and 0.01% SDS. The blot was blocked overnight in 5% milk-TBST at 4°C. The blot was probed with MANDYS8 (1:200, Sigma D8168) and rabbit anti-GAPDH (1:5000, Cell Signaling 2118S). The blot was washed with TBST and probed with mouse or rabbit horseradish peroxidase-conjugated secondary antibodies (Sigma) for 30 min in 5% milk-TBST. Blots were visualized using Western-C ECL substrate (Biorad) on a ChemiDoc chemiluminescent system (Biorad). The full blots are shown in **attached source data.**

Immunofluorescence staining

Skeletal and cardiac muscles were dissected and embedded in OCT using liquid nitrogen-cooled isopentane and stored at −80°C. 10μm sections were cut onto pre-treated histological slides using a cryostat (Leica). Slides were washed in PBS and blocked in PBS supplemented with 5%FBS and 5% goat serum with 0.5% Triton-X 100. Dystrophin was detected with MANDYS8 (1:200, Sigma D8168) in blocking buffer overnight at 4°C. Slides were washed 3x with PBS for 10 min and secondary antibody was applied with DAPI (1:5000) for 30 min at RT. Slides were washed and mounted with ProLong™ Gold Antifade Mountant (Invitrogen) and imaged with an inverted microscope (Leica).

Creatine Kinase assay

Serum creatine kinase (CK) was measured using a Liquid Creatine Kinase Reagent set (Pointe Scientific) following manufacturer's instructions. 5 μL of serum was diluted into 20 μL of sterile PBS and incubated with reagent for 2 minutes and measured by absorbance every minute for 3 readings at 37°C using a nanodrop spectrophotometer set for 340 nm readings. Calculations for total CK in U/L were made according to manufacturer's instructions and plotted relative to levels in serum from wildtype mice.

Recombinant SaCas9 production

A plasmid containing an IPTG-inducible bacterial SaCas9 expression cassette was transformed into Rosetta 2 cells (Millipore EMD) and plated on LB plates with 50 μg/mL Kanamycin and 30 μg/mL Chloramphenicol. Colonies were selected and grown in a starter culture overnight then in a 1L culture for 4–6 hours until OD600 reached 0.6–0.8. The temperature was reduced to 18°C and induced with 0.2 mM IPTG and incubated for 12–16 hours overnight. Cells were isolated and resuspended to 6 mL/g in lysis buffer containing EDTA-free protease inhibitor cocktail (Roche), 1 mM PMSF, and 1 mg/mL lysozyme (Sigma) and kept at 4°C for the remainder of the protocol. Cells were sonicated 10s on and 10s off for 15min. Cell debris was pelleted by centrifugation for 30 min at 16,000xg at 4°C. Protein was isolated with Ni-NTA agarose beads (Qiagen) following manufacturer's instructions. DNA was removed with Sepharose (Sigma) collecting the protein flow through.

The protein was dialyzed overnight at 4°C with 10MWCO dialysis tubing. Protein was concentrated with Vivaspin 20 50kDa MWCO spin filters (GE Healthcare). Samples were aliquoted, flash frozen, and stored at −80°C. Protein was analyzed by protein gel and western blot **(Source data).**

Antibody ELISA

Antibodies against SaCas9 were detected by adapting a protocol from Wang et al., and Chew et al. [7, 43]. Briefly, recombinant SaCas9 protein was diluted in 1x coating buffer (KPL) and used to coat a 96-well Nunc MaxiSorp plate with 0.5 μg of protein per well. Protein was incubated overnight at 4°C to adsorb to the plate. Plates were washed three times for 5 minutes each with 1X wash buffer (KPL). Plates were blocked with 1% BSA blocking solution (KPL) for 1 hour at room temperature. Standard curves for IgG were generated using an αSaCas9 antibody (Diagenode C15200230). Serum samples were added in dilutions ranging from 1:40 to 1:20000 and plates were incubated for 5hrs at 4°C with shaking. Plates were washed 3 times for 5 minutes each and 100 μL of blocking solution containing goat-anti mouse IgG (Sigma 1:4000) was added to each well and incubated at 1hr at room temperature. Plates were washed 4 times for 5 minutes each and 100 μL of ABTS ELISA HRP substrate (KPL) was added to each well. Optical density (OD) at 410nm was measured with a plate reader.

T-Cell ELISPOT

T-cell ELISPOTS were performed as previously described [44]. Briefly, splenocytes from AAV9-SaCas9-injected mice were isolated and purified using Lympholyte M (Cederlane). 250,000 cells were mixed with either Cas9 protein (Applied Biological Materials) or cell media only as a negative control, and subsequently plated in a 96-well ELISPOT plate (Millipore, MSIPS4510) in 100 μL per well. Stimulation was performed with 0.02 μg/μL of Cas9 protein at 37ºC in a humidified incubator, 7% (v/v) CO_2, for 40 h. Mouse IFN-γ ELISPOT pairs (3321–3-250 and 3321–6-250) and Streptavidin-alkaline phosphatase (3310–10) were purchased from Mabtech. Spots were developed using substrate Sigmafast BCIP/NBT (Sigma, B5655). Plates were shipped to Zellnet Consulting and enumerated using a Zeiss KS ELISPOT system. Full plates images are reported in Extended Data Fig. 4.

Statistical Methods and reproducibility

Single comparisons were completed with a Mann-Whitney test with p values reported directly on the figures (Fig 1C, 1E, 2C, 2E). Multiple comparisons were made using Kruskal-Wallis test (Fig. 1I). Two-way ANOVA with post-hoc Tukey test was used to evaluate systemically treated groups with p values reported directly on the figures (Fig 1D, 1F, 2D, 2F). qPCR for gene expression was evaluated by t-test with Holm-Bonferroni multiple comparison correction (Extended Data Fig. 4). All dots plotted are independent biological replicates (individual mice). Information about reproducibility can be found in the Life Sciences Reporting Summary provided with the online version of the manuscript.

Extended data figure legends references [45] [46]

Extended Data

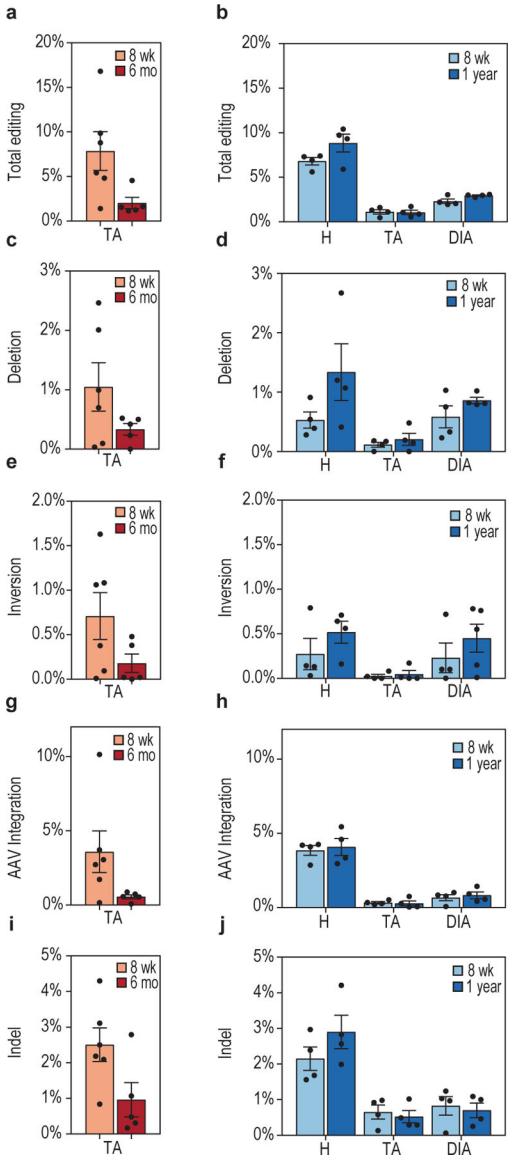

Extended Data Fig. 1. Illumina Nextera-based unidirectional sequencing shows diverse genome changes including deletions, AAV integration, inversions and indel formation.

a, Total editing for local administration. **b**, Total editing for systemic administration in neonates. **c**,**d**, Deletion frequency. **e**,**f**, Inversion frequency. **g**,**h**, AAV integration frequency. **i**,**j**, Indel frequency. Data are mean ± s.e.m. Locally injected mice, $n = 6$; systemically injected mice, $n = 4$.

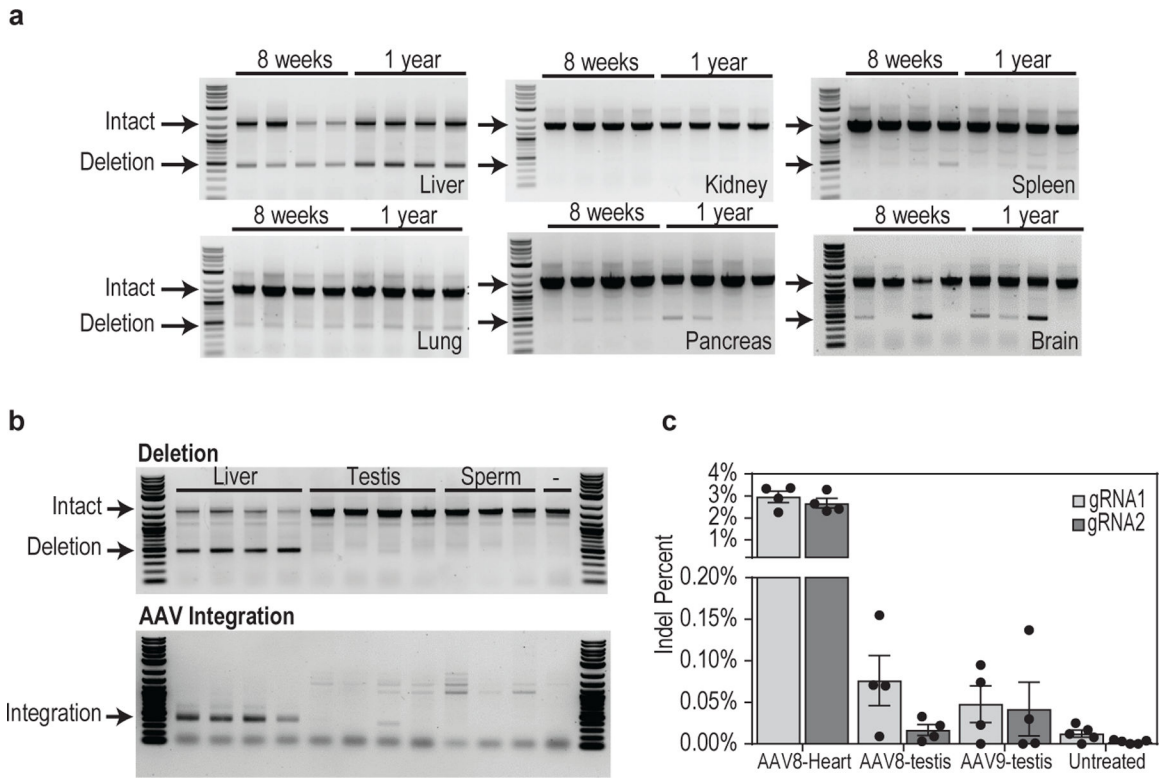

Extended Data Fig. 2. On-target genome editing activity in somatic and germline tissues.

a, Deletion PCR across the dystrophin locus shows Cas9 activity in multiple somatic tissues, including the liver, spleen, lung, pancreas and brain, which all show evidence of targeted gene deletion. There is no detectable deletion in the kidney samples. Cas9 expression is driven by a constitutive CMV promoter. This result is consistent with AAV8 tissue tropism45. The off-target tissue-editing experiment was conducted once. **b**, Deletion PCR of genomic DNA from the testis is mostly negative and undetectable in sperm. AAV integration was only detected in one testis sample and no sperm samples. The germline experiment was conducted once. **c**, Deep sequencing of testis DNA indicates low levels of indel formation for both AAV8- and AAV9-injected mice that were injected as neonates. Data are mean ± s.e.m. $n = 4$ mice in all treated groups; $n = 5$ untreated mice.

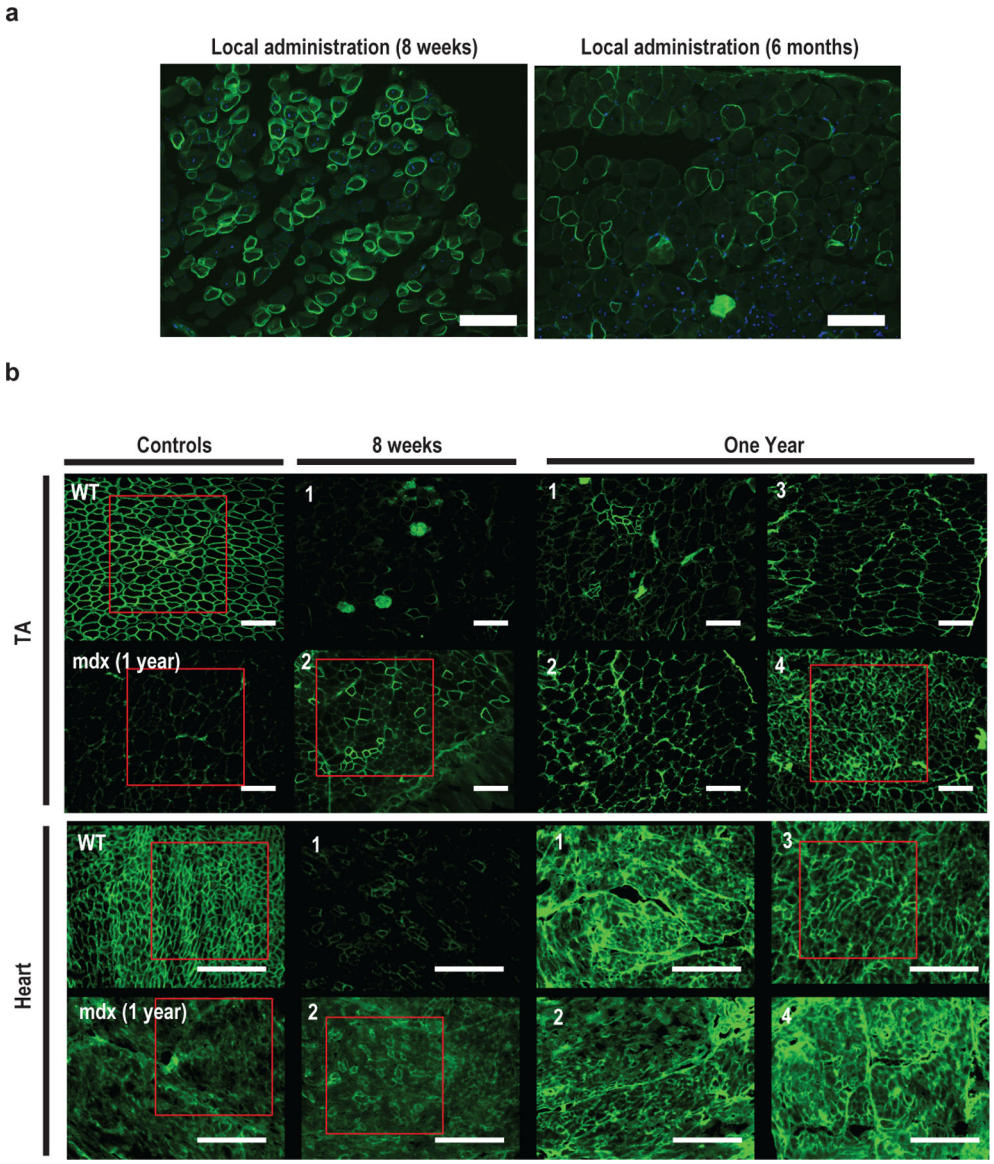

Extended Data Fig. 3. Complete panel of histology shows a decrease in dystrophin staining following local administration and an increase in dystrophin at the 1-year time point in systemically treated mice.

a, The histology images indicate a reduction in dystrophin after local injections, consistent with genomic and transcript data. **b**, Systemic samples show increased dystrophin expression after 1 year. Increased background at the 1-year time point may be a result of fibrosis in the tissue at the later time point. Representative images shown in Fig. 1 are highlighted in red. Scale bars, 200 μm. Dystrophin-restoration experiments were conducted once for each treatment group.

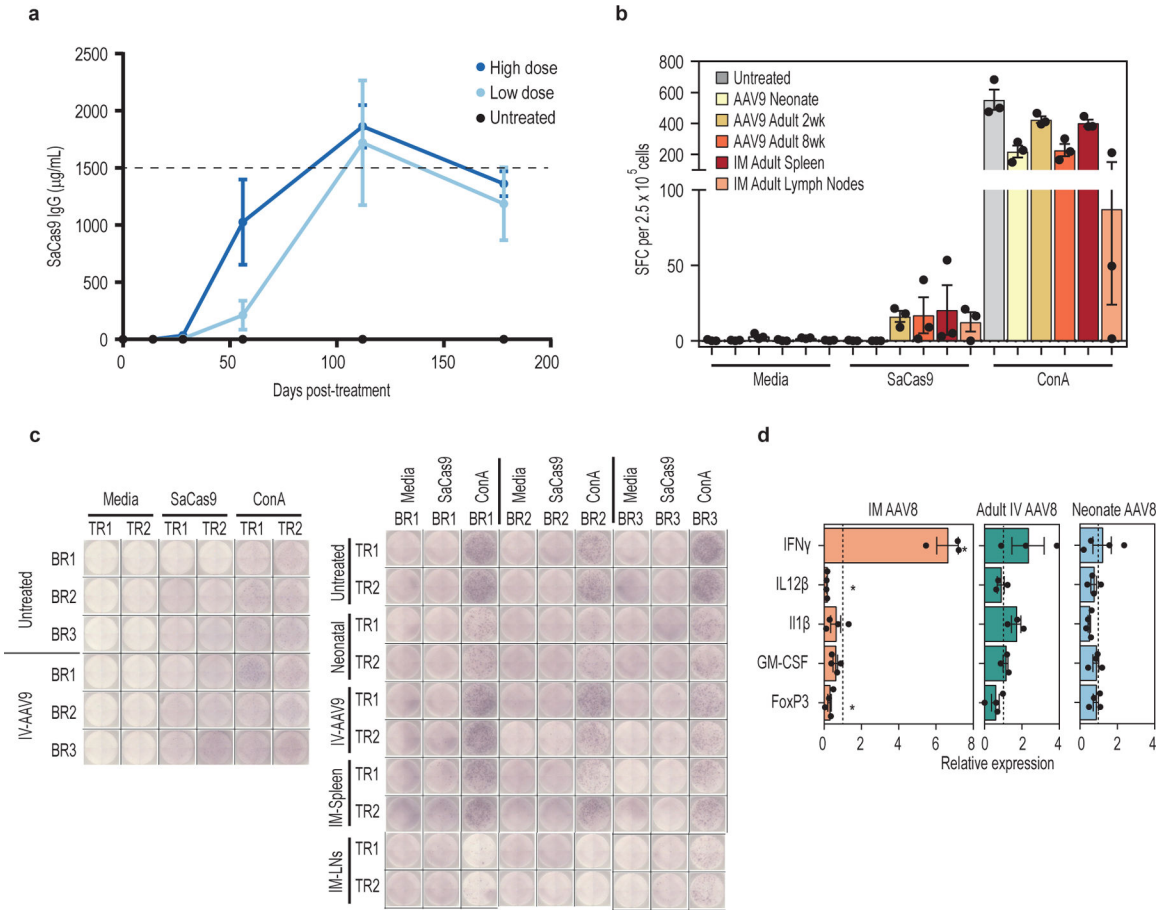

Extended Data Fig. 4. AAV delivery of SaCas9 elicits humoral and cellular immune responses.

a, Mice were administered with an AAV carrying a deactivated, nuclease-null SaCas9 transcriptional repressor (dSaCas9-KRAB) from a related study23. Serum was collected at 4, 8, 16 and 26 weeks. The IgG response invariably developed by 8 weeks in all tested mice and continued to increase until the 16-week time point. Data are mean ± s.e.m. (n = 4 individual mice). The dotted line indicates the end of the linear range of the standard. **b**, ELISpot shows T cell responses in treated adults but not neonates regardless of administration route. Spot-forming cells (SFCs) were detected in mice injected with AAV9-SaCas9 in adults at 2 weeks and 8 weeks after systemic administration, as well as 8 weeks after intramuscular injection. SFCs were not detected in mice treated as neonates. **c**, Complete image panel of ELISpot data. Two separate plates are shown. Data are mean ± s.e.m. n = 3 individual mice, biological replicates (BR) were used with two technical replicates (TR) as individual isolates from each mouse. **d**, Mice administered locally show increased IFNγ and reduced FOXP3 and IL-12β expression, whereas mice administered systemically as adults or neonates show no significant changes. Statistics calculated compared to untreated, t-test with Holm–Bonferroni multiple comparisons correction was used. n = 4, IM-AAV8; n = 3, IV-AAV8; n = 4, Neonate-AAV8.

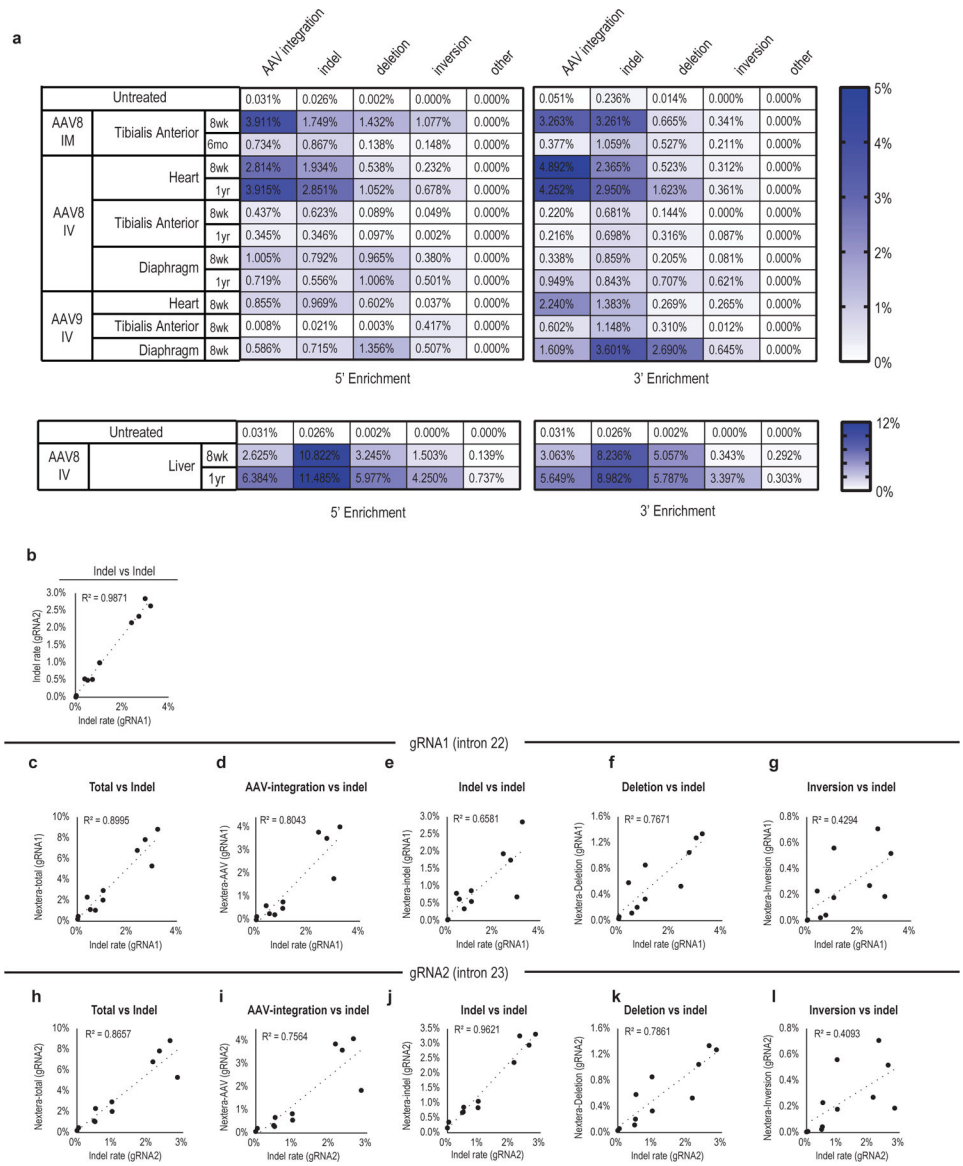

Extended Data Fig. 5. Complete quantitative and reproducibility data for the Illumina Nextera-based unidirectional sequencing measures.

Data associated with Fig. 3b. **a**, Quantitative data for genome-editing measurements are an average of $n = 4$ individual mice. Skeletal and cardiac muscle are shown on a separate scale from liver samples. **b**, Comparison of deep sequencing for both gRNAs. **c**–**g**, Comparison of indel rates for gRNA1 to identify alternate modifications. **h**–**l**, Comparison of indel rates of gRNA2 with alternate modifications. Rare events have poorer correlations. An estimated limit of detection is given based on the inversions detected that range between 0.1% and 0.2%. The limit of detection could be decreased with more input DNA and increased number of reads to detect more rare events, possibly including translocations.

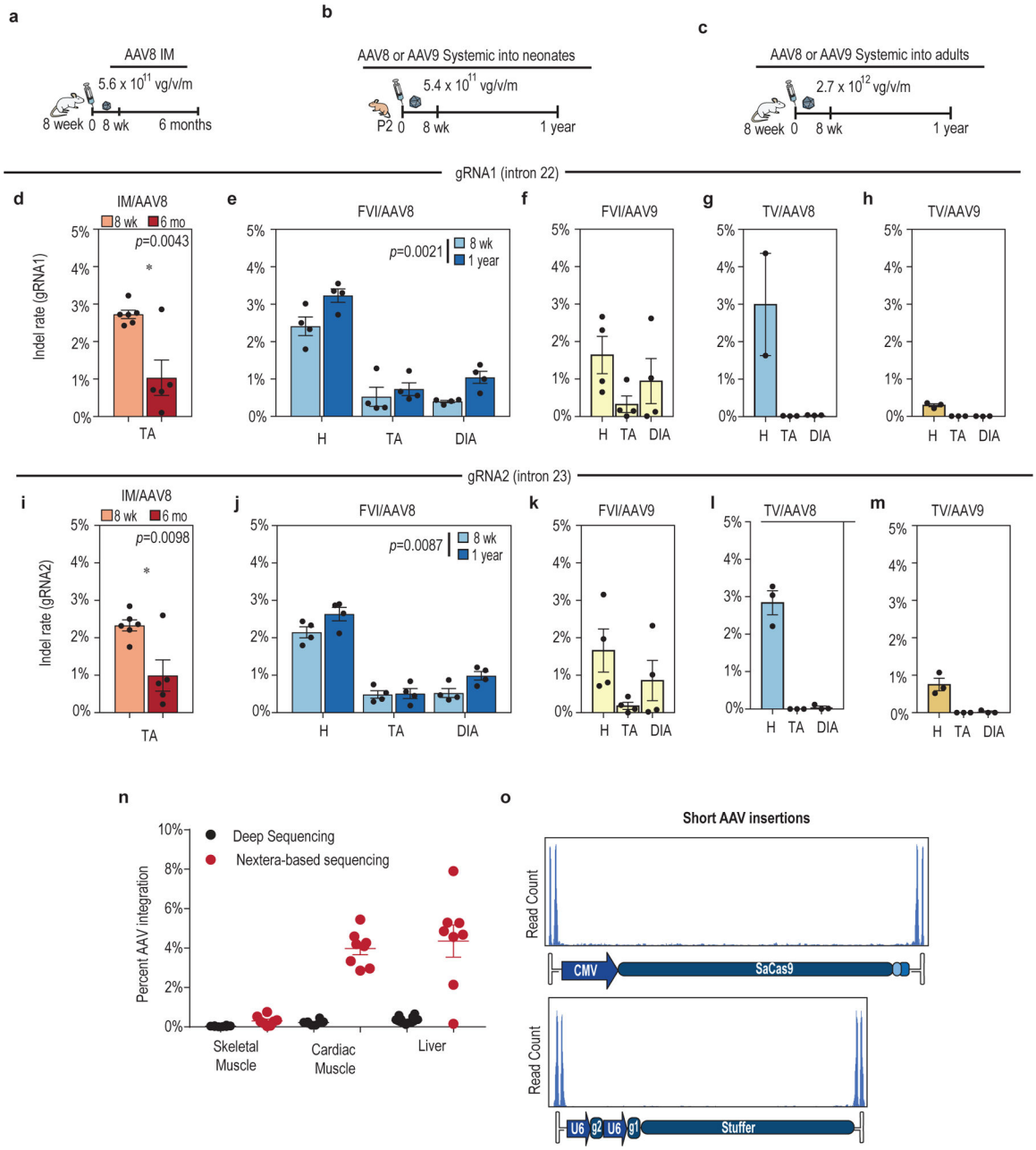

Extended Data Fig. 6. Deep sequencing of target loci for gRNA1 and gRNA2 in multiple tissues and treatment routes show indel formation and short AAV insertions.

a, Mice treated as 8-week-old adults by injection into the tibialis anterior were euthanized and tissues were collected at 8 weeks and 6 months after a single administration. **b**, Systemic administration in neonates by FVI of AAV8 or AAV9 was followed by analysis at 8 weeks and 1 year. **c**, Systemic administration in adults by tail-vein injection was followed by tissue collection at 12 weeks after the administration. **d**, Local administration with AAV8 ($n = 6$, $n = 5$, two-tailed t-test). **e**, Systemic administration with AAV8 in neonates ($n = 4$, two-way ANOVA). **f**, Systemic administration in neonates with AAV9 ($n = 4$). **g**, Tail-vein administration in adults with AAV8 ($n = 3$). **h**, Tail-vein administration in adults with AAV9

(*n* = 3). **i**–**m**, The same administration at the gRNA2 loci. **n**, Small AAV insertions were detected by deep sequencing for insertions that range from 10 to 45 bp in length. These insertions account for a small subset of integrations detected by Nextera-based sequencing. Nextera-based sequencing shows a higher detection rate of AAV genome insertions (*n* = 8). **o**, Short AAV insertions detected by indel sequencing are almost exclusively located within the ITR regions of the AAV vector genome. Data are mean ± s.e.m.

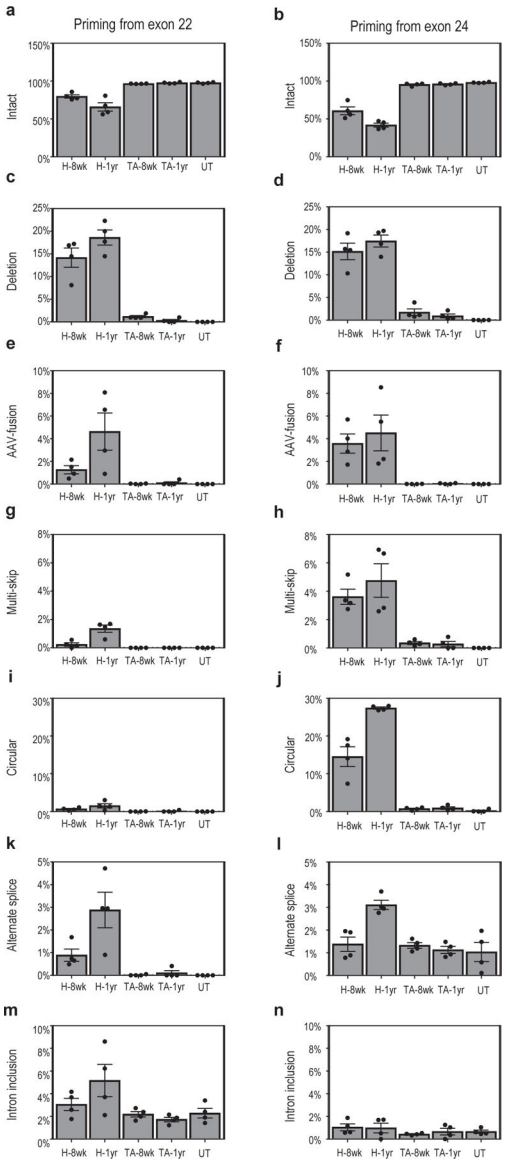

Extended Data Fig. 7. Illumina Nextera-based unidirectional sequencing of cDNA shows transcript changes over time in systemically administered neonates.

There are notable differences in the number of circular RNA events and multi-skipping events when sequencing from the forward or reverse direction, which indicates that alternative splicing may be preferred in reverse direction. a-b) intact unedited transcripts, c-d) exon 23 deleted transcripts, e-f) AAV-fusion transcripts, g-h) transcripts with multiple

skipped exons, i-j) circular transcripts, k-l) transcripts with alternative splicing, m-n) and transcripts with intron inclusion. Data are mean ± s.e.m. (n = 4 for all samples).

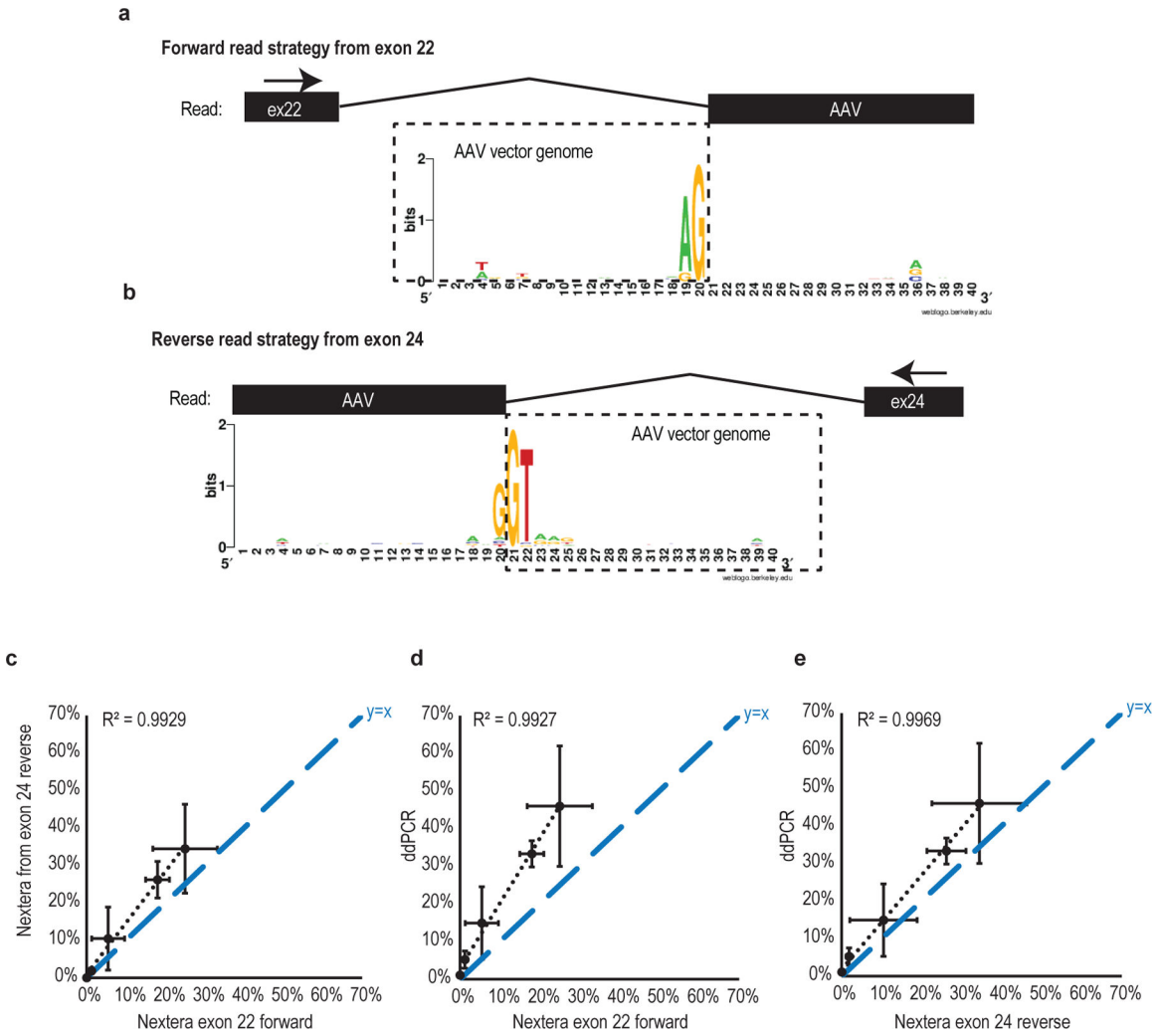

Extended Data Fig. 8. Nextera-based sequencing reveals dystrophin-AAV transcript fusions and is a reproducible method.

a, Web logo map of nucleotide preference for spicing of dystrophin transcript to AAV vector genome shows canonical splicing is preferred. The forward read strategy priming from exon 22 shows that dystrophin-AAV splice fusions prefer an AG as the canonical splice acceptor. The sequencing read is shown as a black box. **b**, Similarly, the reverse priming strategy shows the preference for the canonical GT splice donor before the AAV-dystrophin fusion. The dotted-line box is not in the sequencing read so the AG or GT are revealed by alignment with the vector genome. Web logo maps were generated with the online tool46 at https://weblogo.berkeley.edu. **c**, Deletions as measured by the Nextera method show a higher estimation by the reverse-sequencing method than the forward-sequencing method. **d**,**e**, ddPCR measures higher levels of gene deletion than either Nextera-based strategy. All comparisons were consistent (R^2 > 0.99). The right Nextera-based method had an order of

magnitude higher read count and there is potential bias for transposon recombination. $y = x$ is plotted as a blue dotted line. Data are mean ± s.e.m., all data are from $n = 4$ mice.

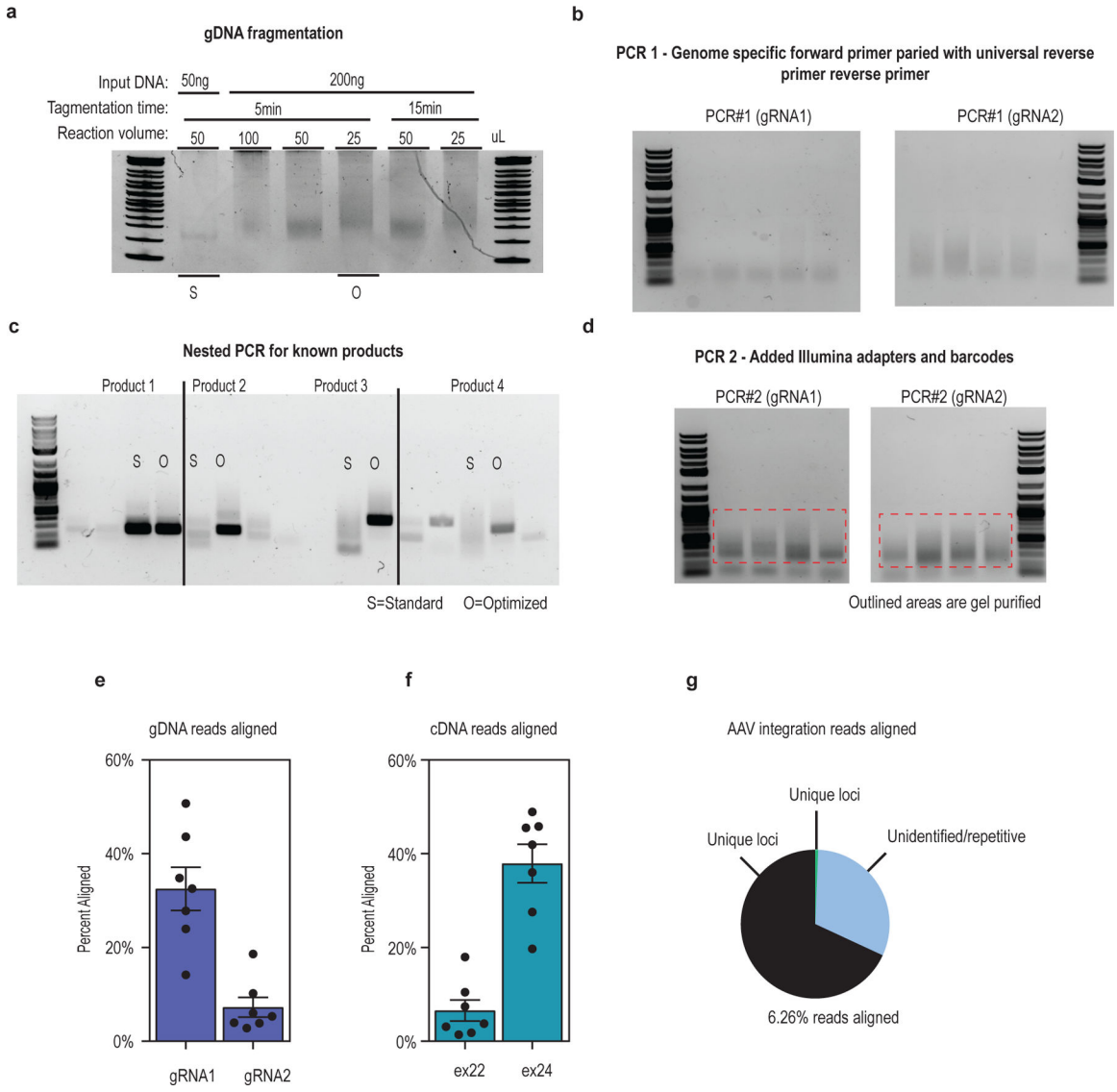

Extended Data Fig. 9. Optimization of the Nextera-based sequencing method.

a, Multiple conditions were tested to find an optimized protocol. The standard method from the manufacturer's protocol is shown as 'S' and the optimized condition that we identified as 'O'. **b**, To test whether the random tagmentation works, a nested PCR was performed after the first PCR. The nested PCR used primer-binding sites of known amplicon size to detect the presence of expected products, including the unmodified target locus and the intended deletion. Only the optimized condition revealed all four predicted amplicons (5′ and 3′ enrichment for both products). We suspect that the standard condition generates fragments that are too short and lose the test-primer-binding site. By contrast, the optimized protocol generates longer DNA fragments that maintain the primer-binding site and would be better suited for unbiased sequencing. Optimization was performed only once. **c**, Gel showing

amplicons after the first PCR. **d**, Gel showing amplicons after adding barcodes and adapters. Bands were purified within the outlined box. Gel images are representative of each sample analysed by deep sequencing (n = 3 independent experiments). **e**, Each method shows varying quantities of reads aligned to the reference because of mispriming. gDNA reads show that the gRNA1–intron22 strategy had a higher percentage of reads aligned to the genome (n = 7). **f**, The cDNA method shows a higher percentage of aligned reads for the exon 24 reverse priming strategy (n = 7). **g**, Sequencing out of the AAV shows 6.26% of reads aligned to the reference with the majority of aligned reads consisting entirely of AAV vector episomes with no novel junctions, represented in black. In blue are reads that did not align to the mouse reference genome or were within repetitive regions that made identification impossible. Green labels indicate the 0.04% of reads that aligned to unique loci within the mouse genome. These reads are listed in detail in Supplemental Table 1, the majority of the reads are in the targeted *Dmd* locus. Data are mean ± s.e.m.

Supplementary Material

Refer to Web version on PubMed Central for supplementary material.

Acknowledgments

This work has been supported by Sarepta Therapeutics, the Allen Distinguished Investigator Program through The Paul G. Allen Frontiers Group, the Muscular Dystrophy Association (grant MDA277360), a Duke–Coulter Translational Partnership Grant, a Duke/UNC-Chapel Hill CTSA Consortium Collaborative Translational Research Award, NIH grant R01AR069085, an NIH Director's New Innovator Award (DP2-OD008586), and the Office of the Assistant Secretary of Defense for Health Affairs, through the Duchenne Muscular Dystrophy Research Program under awards W81XWH-15–1-0469 and W81XWH-16–1-0221. C.E.N. was supported by a Hartwell Foundation Postdoctoral Fellowship and the NIH Pathway to Independence Award (K99EB023979). J.R.H. was supported by a National Science Foundation Graduate Research Fellowship and American Heart Association Predoctoral Fellowship (17PRE33350013).

Works cited

1. Nelson CE, Robinson-Hamm JN, and Gersbach CA, Genome engineering: a new approach to gene therapy for neuromuscular disorders. Nat Rev Neurol, 2017 13(11): p. 647–661. [PubMed: 28960187]
2. Xu L, et al., CRISPR-mediated Genome Editing Restores Dystrophin Expression and Function in mdx Mice. Mol Ther, 2016 24(3): p. 564–9. [PubMed: 26449883]
3. Long C, et al., Genome Editing of Monogenic Neuromuscular Diseases: A Systematic Review. JAMA Neurol, 2016.
4. Nelson CE, et al., In vivo genome editing improves muscle function in a mouse model of Duchenne muscular dystrophy. Science, 2016 351(6271): p. 403–7. [PubMed: 26721684]
5. Tabebordbar M, et al., In vivo gene editing in dystrophic mouse muscle and muscle stem cells. Science, 2016 351(6271): p. 407–11. [PubMed: 26721686]
6. Bengtsson NE, et al., Muscle-specific CRISPR/Cas9 dystrophin gene editing ameliorates pathophysiology in a mouse model for Duchenne muscular dystrophy. Nat Commun, 2017 8: p. 14454. [PubMed: 28195574]
7. Chew WL, et al., A multifunctional AAV-CRISPR-Cas9 and its host response. Nat Methods, 2016 13(10): p. 868–74. [PubMed: 27595405]
8. Flanigan KM, Duchenne and Becker muscular dystrophies. Neurol Clin, 2014 32(3): p. 671–88, viii. [PubMed: 25037084]
9. Hoffman EP, Brown RH Jr., and Kunkel LM, Dystrophin: the protein product of the Duchenne muscular dystrophy locus. Cell, 1987 51(6): p. 919–28. [PubMed: 3319190]

10. Chamberlain JR and Chamberlain JS, Progress toward Gene Therapy for Duchenne Muscular Dystrophy. Mol Ther, 2017 25(5): p. 1125–1131. [PubMed: 28416280]
11. Robinson-Hamm JN and Gersbach CA, Gene therapies that restore dystrophin expression for the treatment of Duchenne muscular dystrophy. Human Genetics, 2016 135(9): p. 1029–1040. [PubMed: 27542949]
12. Dunbar CE, et al., Gene therapy comes of age. Science, 2018 359(6372).
13. Sharma R, et al., In vivo genome editing of the albumin locus as a platform for protein replacement therapy. Blood, 2015.
14. Laoharawee K, et al., Dose-Dependent Prevention of Metabolic and Neurologic Disease in Murine MPS II by ZFN-Mediated In Vivo Genome Editing. Mol Ther, 2018 26(4): p. 1127–1136. [PubMed: 29580682]
15. Amoasii L, et al., Single-cut genome editing restores dystrophin expression in a new mouse model of muscular dystrophy. Sci Transl Med, 2017 9(418).
16. Amoasii L, et al., Gene editing restores dystrophin expression in a canine model of Duchenne muscular dystrophy. Science, 2018 362(6410): p. 86–91. [PubMed: 30166439]
17. Ran FA, et al., In vivo genome editing using Staphylococcus aureus Cas9. Nature, 2015 520(7546): p. 186–U98. [PubMed: 25830891]
18. Kotterman MA and Schaffer DV, Engineering adeno-associated viruses for clinical gene therapy. Nat Rev Genet, 2014 15(7): p. 445–51. [PubMed: 24840552]
19. Spencer MJ, et al., Helper (CD4(+)) and cytotoxic (CD8(+)) T cells promote the pathology of dystrophin-deficient muscle. Clin Immunol, 2001 98(2): p. 235–43. [PubMed: 11161980]
20. Kotterman MA, Chalberg TW, and Schaffer DV, Viral Vectors for Gene Therapy: Translational and Clinical Outlook. Annu Rev Biomed Eng, 2015 17: p. 63–89. [PubMed: 26643018]
21. Brooks AR, et al., Transcriptional silencing is associated with extensive methylation of the CMV promoter following adenoviral gene delivery to muscle. J Gene Med, 2004 6(4): p. 395–404. [PubMed: 15079814]
22. Charlesworth CT, et al., Identification of Pre-Existing Adaptive Immunity to Cas9 Proteins in Humans. bioRxiv, 2018.
23. Thakore PI, et al., RNA-guided transcriptional silencing in vivo with S. aureus CRISPR-Cas9 repressors. Nat Commun, 2018 9(1): p. 1674. [PubMed: 29700298]
24. Hu C and Lipshutz GS, AAV-based neonatal gene therapy for hemophilia A: long-term correction and avoidance of immune responses in mice. Gene Ther, 2012 19(12): p. 1166–76. [PubMed: 22241178]
25. Lee EK, et al., Long-term survival of the juvenile lethal arginase-deficient mouse with AAV gene therapy. Mol Ther, 2012 20(10): p. 1844–51. [PubMed: 22760543]
26. Singh K, et al., Efficient In Vivo Liver-Directed Gene Editing Using CRISPR/Cas9. Mol Ther, 2018 26(5): p. 1241–1254. [PubMed: 29599079]
27. Zhang P, et al., Immunodominant liver-specific expression suppresses transgene-directed immune responses in murine pompe disease. Hum Gene Ther, 2012 23(5): p. 460–72. [PubMed: 22260439]
28. Ferdosi SR, et al., Multifunctional CRISPR/Cas9 with engineered immunosilenced human T cell epitopes. bioRxiv, 2018.
29. Nelson CE and Gersbach CA, Engineering Delivery Vehicles for Genome Editing. Annu Rev Chem Biomol Eng, 2016 7: p. 637–62. [PubMed: 27146557]
30. Giannoukos G, et al., UDiTaS, a genome editing detection method for indels and genome rearrangements. BMC Genomics, 2018 19(1): p. 212. [PubMed: 29562890]
31. Iyombe-Engembe JP, et al., Efficient Restoration of the Dystrophin Gene Reading Frame and Protein Structure in DMD Myoblasts Using the CinDel Method. Molecular Therapy-Nucleic Acids, 2016 5.
32. Kosicki M, Tomberg K, and Bradley A, Repair of double-strand breaks induced by CRISPR–Cas9 leads to large deletions and complex rearrangements. Nature Biotechnology, 2018.
33. Memczak S, et al., Circular RNAs are a large class of animal RNAs with regulatory potency. Nature, 2013 495(7441): p. 333–8. [PubMed: 23446348]

34. Cox DB, Platt RJ, and Zhang F, Therapeutic genome editing: prospects and challenges. Nat Med, 2015 21(2): p. 121–31. [PubMed: 25654603]
35. Miller DG, Petek LM, and Russell DW, Adeno-associated virus vectors integrate at chromosome breakage sites. Nature Genetics, 2004 36(7): p. 767–773. [PubMed: 15208627]
36. Chandler RJ, et al., Vector design influences hepatic genotoxicity after adeno-associated virus gene therapy. J Clin Invest, 2015 125(2): p. 870–80. [PubMed: 25607839]
37. Barzel A, et al., Promoter less gene targeting without nucleases ameliorates haemophilia B in mice. Nature, 2015 517(7534): p. 360–U476. [PubMed: 25363772]
38. Bell P, et al., No evidence for tumorigenesis of AAV vectors in a large-scale study in mice. Molecular Therapy, 2005 12(2): p. 299–306. [PubMed: 16043099]
39. Donsante A, et al., AAV vector integration sites in mouse hepatocellular carcinoma. Science, 2007 317(5837): p. 477. [PubMed: 17656716]
40. Gil-Farina I, et al., Recombinant AAV Integration Is Not Associated With Hepatic Genotoxicity in Nonhuman Primates and Patients. Mol Ther, 2016 24(6): p. 1100–1105. [PubMed: 26948440]
41. Gombash Lampe SE, Kaspar BK, and Foust KD, Intravenous injections in neonatal mice. J Vis Exp, 2014(93): p. e52037. [PubMed: 25407048]
42. Pinello L, et al., Analyzing CRISPR genome-editing experiments with CRISPResso. Nat Biotechnol, 2016 34(7): p. 695–7. [PubMed: 27404874]
43. Wang D, et al., Adenovirus-mediated somatic genome editing of Pten by CRISPR/Cas9 in mouse liver in spite of Cas9-specific immune responses. Hum Gene Ther, 2015.
44. Chen J, et al., The use of self-adjuvanting nanofiber vaccines to elicit high-affinity B cell responses to peptide antigens without inflammation. Biomaterials, 2013 34(34): p. 8776–8785. [PubMed: 23953841]
45. Zincarelli C, et al., Analysis of AAV serotypes 1–9 mediated gene expression and tropism in mice after systemic injection. Mol Ther, 2008 16(6): p. 1073–80. [PubMed: 18414476]
46. Crooks GE, et al., WebLogo: a sequence logo generator. Genome Res, 2004 14(6): p. 1188–90. [PubMed: 15173120]

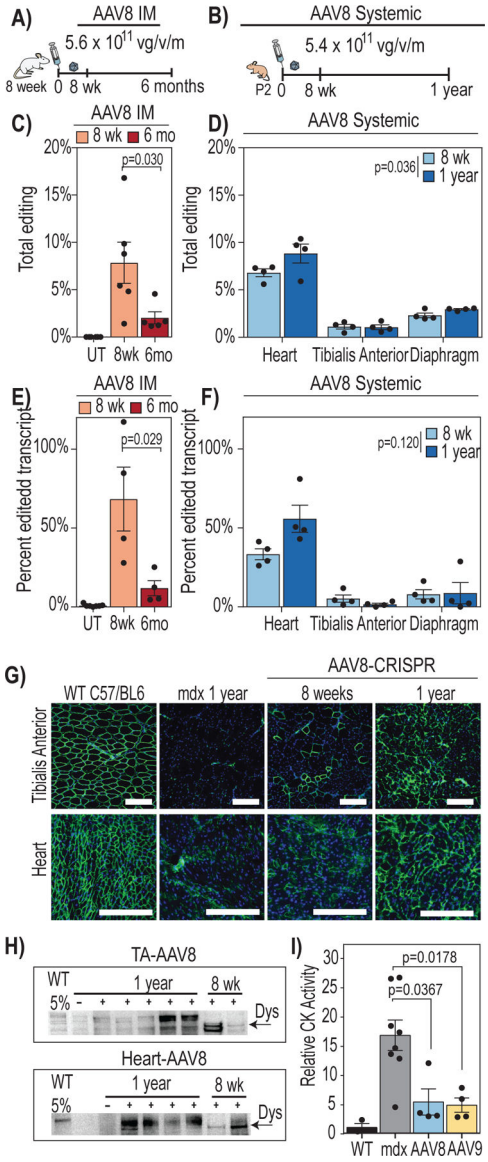

Figure 1–. Genome editing is sustained for one year in neonatal mice treated by intravenous administration.

A) Mice were treated as adults by AAV injection into the tibialis anterior or B) systemically by facial vein injection as neonates. C) Quantification of total gene modification shows a significant decrease over 6 months following local administration (n=6, 8 wk; n=5, 6 mo, one-sided t-test) and D) a significant increase in neonates treated systemically (n=4, two-way ANOVA). E) ddPCR shows the same trend for deletion of exon 23 from the transcript for local injections (n=4, one-sided t-test) and F) systemic injections (n=4, two-way ANOVA). G) Dystrophin expression is sustained in cardiac muscle and skeletal muscle one year after systemic administration into neonates (scale = 200μm). Histological images are available as source data. H) Western blot confirms the presence of dystrophin in skeletal and cardiac muscle. Full uncropped blots and are available in as source data. I) After 8 weeks, systemically treated neonatal mice show a significant decrease in creatine kinase (n=3, WT;

n=8, untreated; *n*=4, treated; one-way ANOVA with multiple comparisons correction). Bar graphs are reported as mean ± SEM.

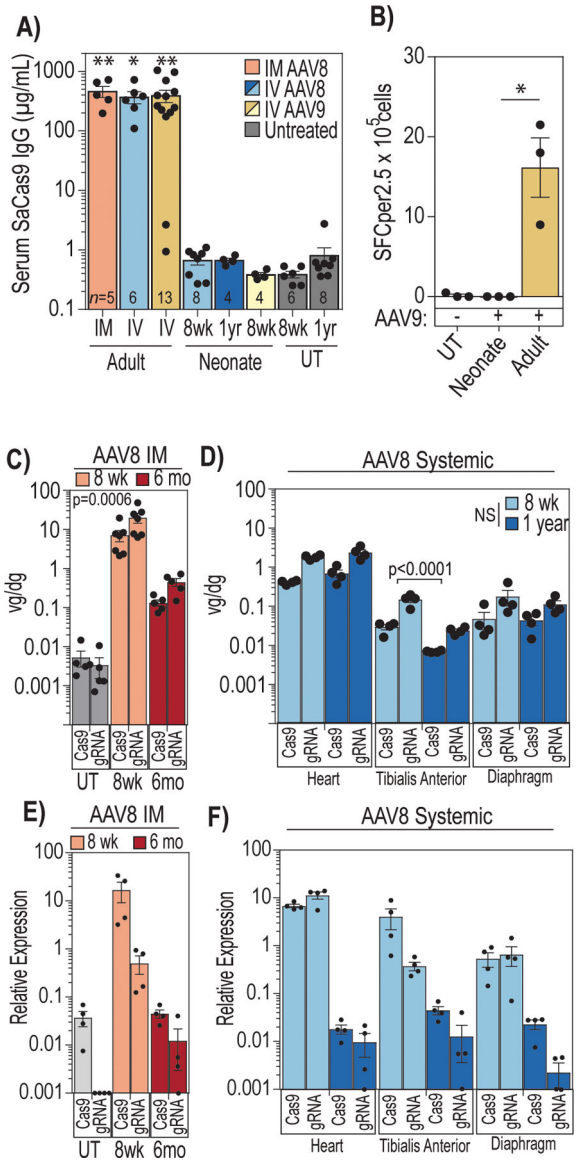

Figure 2–. Host response to AAV-CRISPR for DMD.

A) Antibodies against SaCas9 are detected in mice treated as adults but not in mice treated as neonates after eight weeks or one year (one-way ANOVA with multiple comparisons *p<0.05, **p<0.01 compared with UT-8wk, *n* indicated on graph). B) Mice injected as adults with AAV encoding Cas9 have T cells that are stimulated by exposure to SaCas9 to produce IFNγ as shown by ELISPOT (One-sided t-test, p=.0246, *n*=3 each condition, SFC = spot forming colony). C-D) A significant loss in total AAV vector genomes per diploid genome (vg/dg) is detected in skeletal muscle following intramuscular injection and intravenous injection but not in cardiac muscle and diaphragm (2-way ANOVA with Tukey's multiple comparisons test, *n*=7, IM-8wk; *n*=5 IM-6mo, *n*=4 all systemic groups). E-F) Expression of both the Cas9 mRNA and gRNAs dissipates between the early and late time points. Skeletal muscle also shows lower gRNA expression than cardiac muscle (2-way

ANOVA with Tukey's multiple comparisons test, (n=4, all groups). Bar graphs are reported as mean ± SEM.

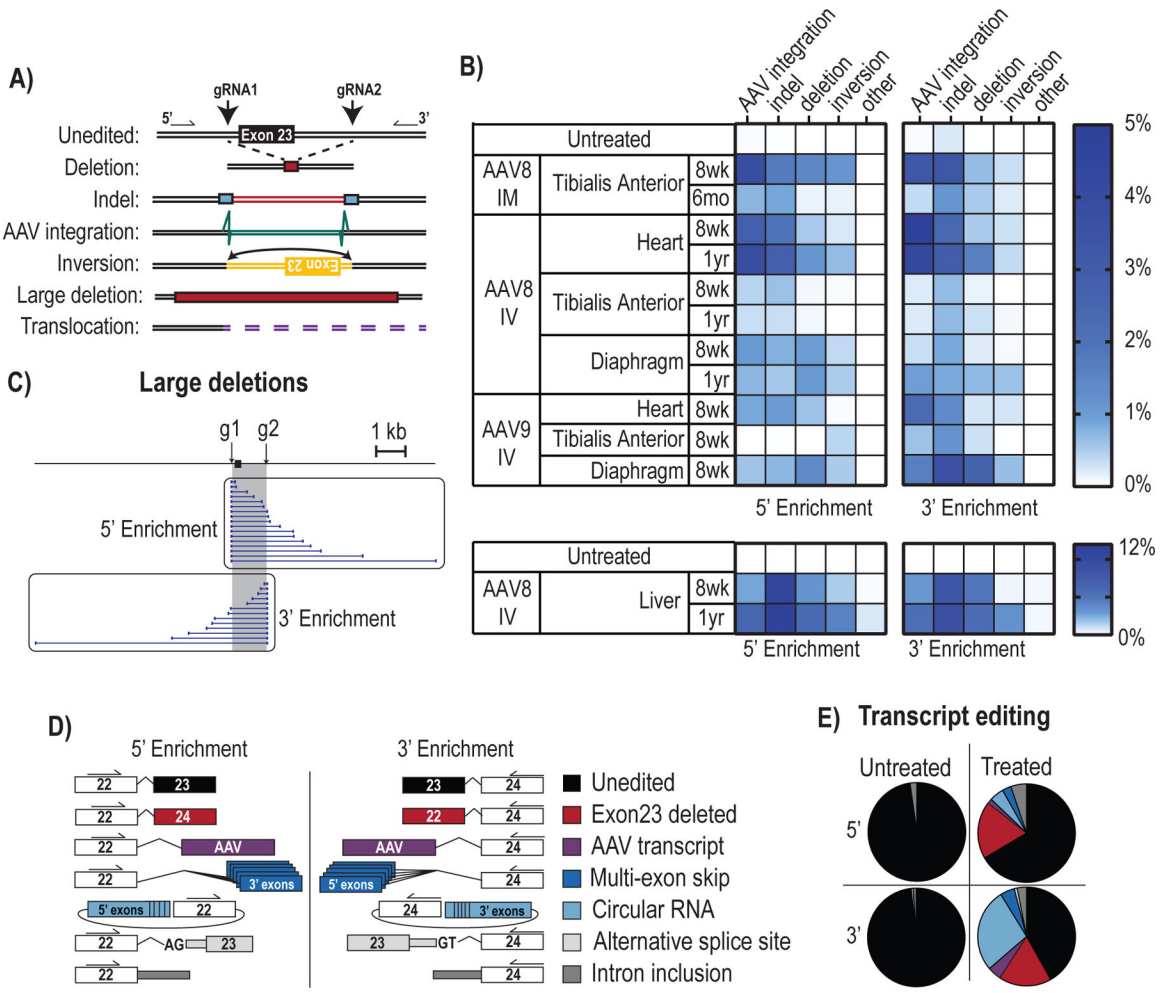

Figure 3–. In vivo genome editing generates diverse on-target genome modifications including AAV integrations and aberrant splicing.

A) Potential on-target genomic changes resulting from targeted DNA cleavage are shown schematically. B) Unbiased analysis of the target site in multiple tissues after administration of AAV-CRISPR quantifies the level of each category of editing events. C) Large deletions around the target site were detected in the liver of mice treated with AAV8. D) Unbiased sequencing applied to the cDNA showed diverse transcript outcomes including aberrant splicing as shown schematically. E) Data from extracted cardiac muscle 8 weeks after administration shows the proportion of transcript editing events. Data for panel B and D were n=4 individual mice for treated and untreated.

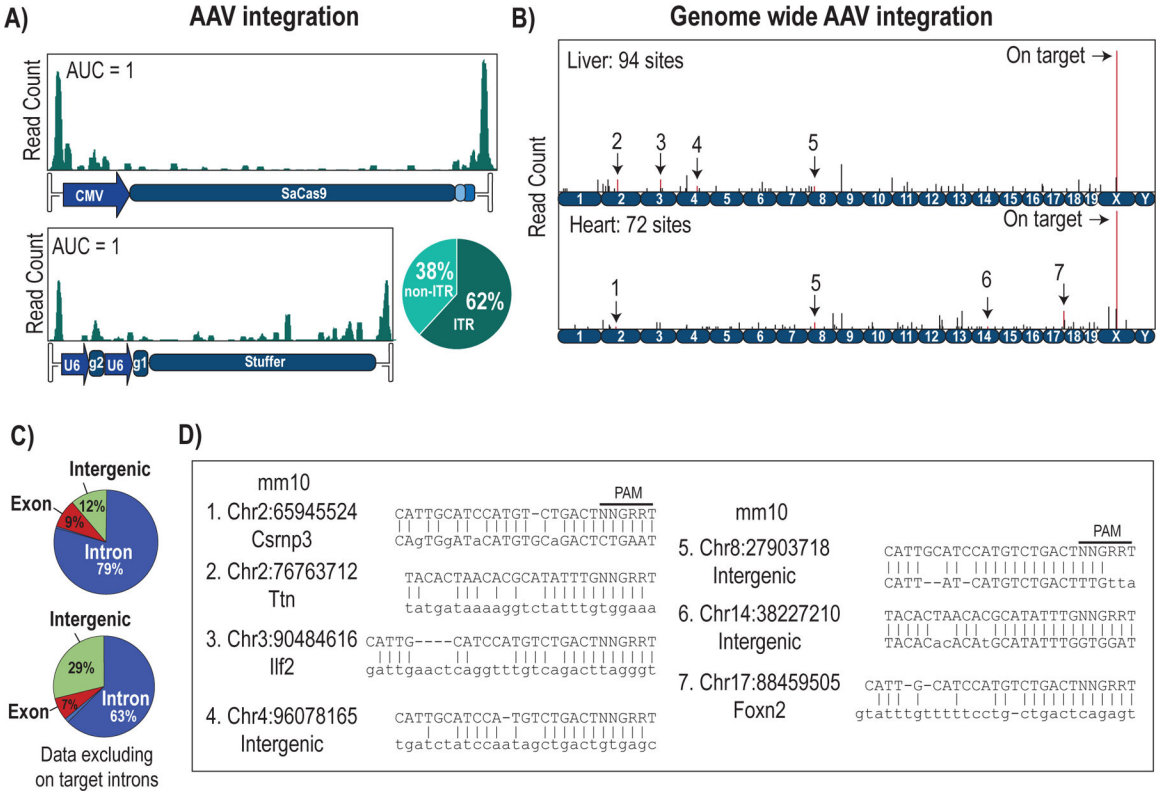

Figure 4- AAV integrations into *Dmd* locus and genome-wide.

A) AAV integrations were detected in the gRNA target sites. 62% of integrations occurred within the ITRs and the remaining 38% occurred within the viral genome. B) A similar approach was used to map AAV integrations genome-wide in both the liver and heart eight weeks after systemic administration to neonatal mice. The top hits include the two gRNA target sites flanking exon 23 of the *Dmd* gene, but numerous other AAV integration sites were detected. C) Genome-wide AAV integration sites were primarily located within introns of genes. D) Possible sites of CRISPR off-target activity were identified by searching for sequences similar to the intended gRNA on-target site nearby the recovered genomic AAV integrations.